Thermodynamic Assessment of the Mn-O System

MINGSHENG WANG and BO SUNDMAN

A thermodynamic assessment of the Mn-O system has been made by using thermodynamic models for the Gibbs energy of individual phases. A set of evaluated thermodynamic parameters was obtained by considering the available experimental information, and it gives a reasonable description of the system. The thermodynamic parameters of the system and comparisons between the calculation and experimental measurements, including phase diagrams, are presented.

I. INTRODUCTION

THE phase diagram of the Mn-O system was recently evaluated by Massalski *et al.*,[1] mainly based on the reported information of Trömel *et al.*[2] and Chen.[3] The system exhibits a wide liquid miscibility gap on the Mn-$Mn_{1-x}O$ side and an eutectic point on the $Mn_{1-x}O$-Mn_3O_4 side.[1-4] The manganosite ($Mn_{1-x}O$) is a nonstoichiometric compound with a deficit of Mn. The reported experimental information on the phase diagram is rather scarce and imprecise. However, many thermodynamic investigations have been reported in the literature dealing with various aspects of pure manganese and manganese oxides. The purpose of the present assessment is to obtain a set of revised thermodynamic descriptions of various phases and a thermodynamically consistent phase diagram of the Mn-O system based on the relevant experimental information by means of the CALPHAD technique.

II. EXPERIMENT INFORMATION

The available experimental information on the Mn-O system has been reviewed in the present work. Table I shows the crystal structure data of the solid phases.

A. *Manganese (Mn)*

The thermodynamic properties of condensed manganese have been compiled several times.[5-10] The most recent result by Guillermet *et al.*[10] was adopted in the present assessment.

B. *Manganosite ($Mn_{1-x}O$)*

Manganosite is a nonstoichiometric compound with the halite type of crystal structure. The oxygen activity has been measured by several authors,[11-14] but the deviations among these results are large. Bransky and Tallan[13] measured the excess oxygen in $Mn_{1-x}O$ in the temperature range of 1273 to 1773 K and at oxygen pressures of 10^{-14} to 1 atm by the thermogravimetric method. However, the excess oxygen that they measured is rather small, especially at the temperatures of 1273 and 1373 K. This may be due to an incorrect assumption regarding the evaporation rate of manganosite during the experiment. Janowski *et al.*[14] also studied the excess oxygen by the same method, but the calculated oxygen pressure of the gas phase was too low to keep the manganosite thermodynamically stable. Davies and Richardson[11] studied the excess oxygen of manganosite by analyzing the composition of the samples quenched from a certain temperature and oxygen pressure. The experimental data are probably rather imprecise, because they found that oxygen pressure in equilibrium with manganosite only varies with the oxygen composition of manganosite but does not change with temperature from 1773 to 1923 K. In 1974, Picard and Gerdanian,[12] with an improved thermogravimetric technique, measured the oxygen activity at temperatures of 1273, 1323, 1373, and 1423 K. In the present assessment, only Picard's experimental data were used in the optimization, because they gave better agreement with the experimental data of the oxygen solubility in manganosite equilibrated with Mn_3O_4 reported by Fender and Riley.[15] Information on the Gibbs energy of formation of manganosite, using a solid electrolyte galvanic cell, obtained by Schwerdtfeger[16] and Simeonov *et al.*,[17] was accepted. The heat capacity was studied by Kleinclaus *et al.*[18] in the temperature range from 20 to 700 K, and some data from 298 to 700 K were used in the optimization. The heat content measured by Southard and Shomate[19] was adopted, and $\Delta^\circ H_{298}$ and $^\circ S_{298}$ were taken from the selected values by Kubaschewski *et al.*[20]

C. *Hausmanite (Mn_3O_4)*

Hausmanite is considered as a stoichiometric compound in the present work. Several authors[22-29] measured the equilibrium oxygen pressure of hausmanite and manganosite, and the experimental data reported by Schaefer,[22] Ramana Rato and Tare[23] and Price and Wagner[24] were used in the optimization. The experimental data of the heat capacity and $^\circ S_{298}$ measured by Robie and Hemingway,[30] the heat content from 763 to 1768 K studied by Southard and Moore,[31] and $\Delta^\circ H_{298}$ from Kubaschewski *et al.*[20] were also used. There are several reports[20,23,31-35] about the values of temperature and enthalpy of a structural transformation from α-Mn_3O_4 to β-Mn_3O_4, and not all of them agree. The values of ΔH = 20,810 J/mol and T = 1445 K, according to a number of measurements,[20,23,32,33] were accepted.

MINGSHENG WANG, formerly Research Associate, Royal Institute of Technology, Stockholm, Sweden, is Lecturer, on leave from the Department of Metallurgical Engineering, Baotou Institute of Iron and Steel Technology, Baotou, People's Republic of China. BO SUNDMAN, Docent of Physical Metallurgy, is with the Division of Physical Metallurgy, Royal Institute of Technology, S-100 44 Stockholm, Sweden.

Manuscript submitted May 4, 1992.

Table I. Crystal Structure Data

Phase	Pearson Symbol	Space Group	Strukturbericht Designation	Prototype	Reference
δ-Mn	cI2	$Im\bar{3}m$	A2	W	1
γ-Mn	cF4	$Fm\bar{3}m$	A2	Cu	1
β-Mn	cP20	$P4_132$	A13	βMn	1
α-Mn	cI58	I43m	A12	αMn	1
MnO	cF8	$Fm\bar{3}m$	B1	NaCl	1
β-Mn_3O_4	cF56	$Fd\bar{3}m$	$H1_1$	—	21
α-Mn_3O_4	tI28	$I4_1/amd$	—	—	21
Mn_2O_3	cI80	Ia3	—	—	21
MnO_2	tP6	$P4_2/mnm$	C4	TiO_2	21

D. *Bixbyite (Mn_2O_3)*

Bixbyite also exists in at least two polymorphic forms, as pointed out as early as 1934 by Dubois.[36] One form, generally called α, has a body-centered cubic (bcc) structure, while the other, generally called γ, has a spinel structure. According to Masson,[37] the α form is stable relative to the γ form under all conditions. The γ form was thus not considered in the present work. For the assessment of the Gibbs energy of Mn_2O_3, the following experimental information was used. The heat capacity from 299 to 345 K and $^\circ S_{298}$ were measured by Robie and Hemingway,[30] the heat content from 397 to 1698 K was studied by Orr,[38] and the Gibbs energy of formation of α-Mn_2O_3 from Mn_3O_4 and oxygen was taken from the experimental measurements by Schaefer,[22] Chen and Chen[39] and Huebner and Sato.[28] The value of $\Delta^\circ H_{298}$ is from Kubaschewski *et al.*[20]

E. *Pyrolusite (MnO_2)*

There are large deviations among the experimental measurements of the oxygen pressure in equilibrium with Mn_2O_3 and MnO_2.[25,40–43] Because the oxidation of Mn_2O_3 to MnO_2 is very slow at ordinary pressure, most of the experimental measurements concerned were carried out from the decomposition process of MnO_2, but it has been extremely difficult to attain the actual equilibrium conditions. According to a recent experimental investigation by Chen and Chen,[39] the generally accepted data reported by Otto[40] are the most reliable ones and they were now used, together with the reported values of the heat capacity from 298 to 376.5 K and $^\circ S_{298}$ by Robie and Hemingway,[30] the heat content from 407 to 778 K by Moore,[44] and $\Delta^\circ H_{298}$ from Kubaschewski *et al.*[20]

F. *Liquid*

The experimental information on the liquid phase is rather limited. The temperature of the invariant equilibria were mainly taken from Trömel *et al.*,[2] except for the eutectic temperature of manganese and manganosite which was from Chen.[3] The available manganosite solubility in liquid manganese was taken from the experimental measurements by Jacob[45] and Simeonov *et al.*[17]

G. *α-, β- and γ-Mn*

There is no experimental information available on the oxygen solubility in the α-, β- and γ-Mn phases, and these were treated as pure.

III. THERMODYNAMIC MODELS

The compound-energy model developed by Hillert and co-workers[46–49] has been successfully applied to metal oxide systems.[50,51] A detailed thermodynamic description of the model used in the Fe-O system is provided by Sundman.[50] In the present work, the two-sublattice model is used for the manganosite ($Mn_{1-x}O$) phase and the liquid phase, and the description of the model is the same as the one used in the Fe-O system.[50] Hausmanite (Mn_3O_4), bixbyite (Mn_2O_3), and pyrolusite (MnO_2) are considered as stoichiometric compounds. The Gibbs energy of these compounds is represented as a function of temperature with five parameters.

A. *Manganosite*

According to many studies,[2,11–14] manganese in the manganosite (halite) phase exists in two ionic states, Mn^{+2} and Mn^{+3}, and the fraction of Mn^{+3} increases with the oxygen potential and temperature, but some authors[3,12] also reported the existence of the Mn^{+1}. In the present assessment, only Mn^{+2} and Mn^{+3} ions are considered. The ideal structure of halite is a simple face-centered cubic (fcc) arrangement of oxygen ions, containing manganese ions in the octahedral interstitial sites. In order to accommodate the trivalent manganese ions, vacant sites are introduced in the octahedral sublattice. Taking this into account, the halite phase may be represented with the following formula:

$$(Mn^{+2}, Mn^{+3}, Va)_1(O^{-2})_1$$

The phase can be represented in a constitutional triangle, and its physical significance was discussed by Sundman.[50] The compound energy model gives the expression of the Gibbs energy as follows:

$$G_m = y_2{}^\circ G_{2O} + y_3{}^\circ G_{3O} + y_V{}^\circ G_{VO} + RT \cdot [y_2 \ln(y_2) + y_3 \ln(y_3) + y_V \ln(y_V)] + {}^E G_m \quad [1]$$

where the y_2 and y_3 are the fractions of sites in the metallic sublattice occupied by divalent and trivalent manganese ion, respectively, and y_V is the fraction of vacant sites. The y_i fractions are usually called site fractions. The three $^\circ G$ terms describe the Gibbs energy of stoichiometric MnO and hypothetical ionic compounds MnO^{+1} and O^{-2}, respectively. According to Sundman,[50] the parameter $^\circ G_{VO}$ is set to zero for convenience.

The excess Gibbs energy, ${}^{E}G_m$, for the halite is described with a Redlich-Kister expression of two terms:

$$\begin{aligned}{}^{E}G_m = {} & y_2 y_3[L^0_{2,3:O} + (y_2 - y_3)L^1_{2,3:O}] \\ & + y_2 y_V[L^0_{2,V:O} + (y_2 - y_V)L^1_{2,V:O}] \\ & + y_3 y_V[L^0_{3,V:O} + (y_3 - y_V)L^1_{3,V:O}] \end{aligned} \quad [2]$$

In the interaction parameters, a colon (:) is used to separate constituents in different sublattices, whereas a comma (,) is used to separate constituents in the same sublattice. In order to extrapolate to a multicomponent system, all parameters involving vacancies introduced for electroneutrality are set to zero. The relation between the mole fraction and the site fraction is expressed by the following formulas:

$$x_{Mn} = \frac{y_2 + y_3}{1 + y_2 + y_3} \quad [3]$$

$$x_O = \frac{1}{1 + y_2 + y_3} \quad [4]$$

Due to the condition of electroneutrality, the maximum value for y_3 is 2/3, and the model for the halite phase can describe the contents of oxygen x_O from 0.5 to 0.6.

B. *Liquid*

For the liquid phase, the ions Mn^{+2}, Mn^{+3}, O^{-2}, and vacancies with an induced charge are considered, and the ionic two-sublattice model[49] was adopted, which assumes that there is one sublattice for anions and one for cations and hypothetical vacancies. The formula can thus be written as

$$(Mn^{+2}, Mn^{+3})_P(O^{-2}, Va^{-Q})_Q$$

According to the model, the stoichiometric coefficients P and Q vary with the composition in order to make the phase electrically neutral, *i.e.*:

$$P = \sum_i y_i(-v_i) + y_{Va}Q$$

$$Q = \sum_j y_j v_j \quad [5]$$

where v_i is the valence of anion i and v_j the valence of cation j.

The Gibbs energy expression used for the liquid is

$$\begin{aligned} G_m = {} & y_2 y_O {}^{\circ}G_{Mn_2O_2} + y_3 y_O {}^{\circ}G_{Mn_2O_3} \\ & + Q(y_2 y_V {}^{\circ}G_{Mn^{+2}:V^{-2}} + y_3 y_V {}^{\circ}G_{Mn^{+3}:V^{-3}}) \\ & + PRT[y_2 \ln(y_2) + y_3 \ln(y_3)] \\ & + QRT[y_O \ln(y_O) + y_V \ln(y_V)] + {}^{E}G_m \end{aligned} \quad [6]$$

The first and second terms contain the Gibbs energy of 2 moles of MnO and 1 mole Mn_2O_3, respectively. The third term is the Gibbs energy of pure manganese. The fourth term represents a hypothetical liquid Mn in an excited state. The excess Gibbs energy term, ${}^{E}G_m$, with two Redlich-Kister terms, is

$$\begin{aligned}{}^{E}G_m = {} & y_2 y_3 y_V[L^0_{2,3:V} + (y_2 - y_3)L^1_{2,3:V}] \\ & + y_2 y_3 y_O[L^0_{2,3:O} + (y_2 - y_V)L^1_{2,3:V}] \\ & + y_2 y_O y_V[L^0_{2:O,V} + (y_O - y_V)L^1_{2:O,V}] \\ & + y_3 y_O y_V[L^0_{3:O,V} + (y_O - y_V)L^1_{3:O,V}] \end{aligned} \quad [7]$$

The four sets of interaction parameters represent the sides of a reciprocal system. However, $L^0_{2,3:V}$, $L^1_{2,3:V}$, $L^0_{3:O,V}$, and $L^1_{3:O,V}$ are put to zero, because they are important only far from the composition of the stable liquid phase and cannot be evaluated with any certainty. The remaining four interaction parameters were used to fit the experimental data.

IV. RESULTS AND DISCUSSION

The assessment was carried out by using the computer software PARROT, developed by Jansson,[52] included in the Thermo-Calc databank system.[53] The evaluated parameters of the various phases are listed in Table II, and the calculated phase diagram at 0.21 atm of oxygen is shown in Figure 1. A list of invariant equilbria is given in Table III, and the calculated values of $\Delta^{\circ}H_{298}$ and ${}^{\circ}S_{298}$ of various compounds are shown in Table IV and compared with the values from literature.

A. *Manganosite*

The assessment began with stoichiometric manganosite. The calculated heat content and Gibbs energy of formation fit well with the experimental data, which are shown in Figures 2 and 3. Much attention was then paid to reproduce the oxygen activity as a function of composition. The final accepted results are plotted in Figure 4(a) and compared with the experimental data by

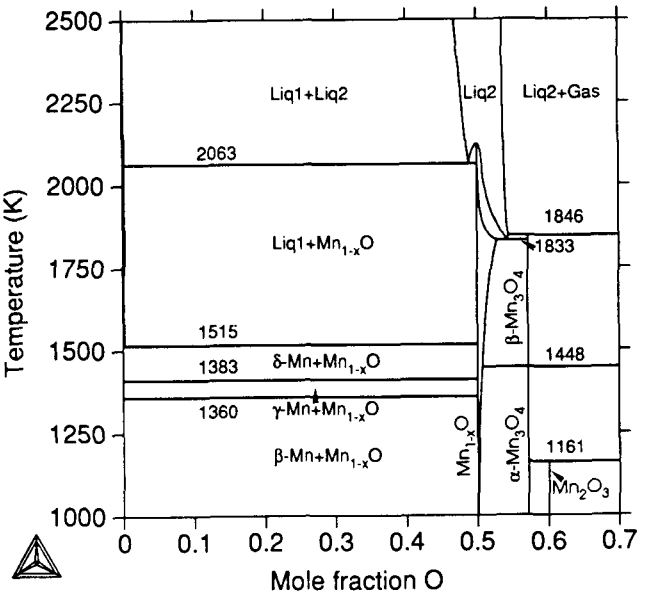

Fig. 1—Calculated Mn-O phase diagram at 0.21 atm of oxygen.

Table II. Summary of the Parameters Describing the Thermodynamic Properties of the MnO-System (Values are in SI Units)

The magnetic contribution to Gibbs energy is described by

$G_m^{mo} = RT \ln(\beta + 1) f(\tau)$, $\tau = T/Tc$

For $\tau < 1$: $f(\tau) = 1 - \left[\frac{79\tau^{-1}}{140p} + \frac{474}{497}\left(\frac{1}{p} - 1\right)\left(\frac{\tau^3}{6} + \frac{\tau^9}{135} + \frac{\tau^{15}}{600}\right)\right] \Big/ A$

For $\tau > 1$: $f(\tau) = -\left(\frac{\tau^{-5}}{10} + \frac{\tau^{-15}}{315} + \frac{\tau^{-25}}{1500}\right) \Big/ A$

where $A = \left(\frac{518}{1125}\right) + \left(\frac{11{,}692}{15{,}975}\right)$

$\left[\left(\frac{1}{p}\right) - 1\right]$ and p depends on the structure.

Gas (O_2)

Constituents O_2

${}^{\circ}G_{O_2}^{GAS} - H_{O_2}^{SER} = +G(O_2, gas) + RT \ln P$

Ionic-liquid

2 sublattices, sites 2:2

Constituents Mn^{+2}, Mn^{+3}:O^{-2}, Va

${}^{\circ}G_{Mn^{+2}:O^{-2}}^{IONIC\text{-}LIQ} - 2H_{Mn}^{SER} - 2H_O^{SER} = +2G(MnO, liq)$

${}^{\circ}G_{Mn^{+3}:O^{-2}}^{IONIC\text{-}LIQ} - 2H_{Mn}^{SER} - 3H_O^{SER} = +2.5G(MnO, liq) - 390{,}784 + 291.8765T$

${}^{\circ}G_{Mn^{+2}:Va}^{IONIC\text{-}LIQ} - H_{Mn}^{SER} = +G(Mn, liq)$

${}^{\circ}G_{Mn^{+3}:Va}^{IONIC\text{-}LIQ} - H_{Mn}^{SER} = +G(Mn, liq) + 87{,}028$

${}^{0}L_{Mn^{+2}:O^{-2},Va}^{IONIC\text{-}LIQ} = +186{,}771 - 12.9648T$

${}^{1}L_{Mn^{+2}:O^{-2},Va}^{IONIC\text{-}LIQ} = +219{,}594 - 132.928T$

${}^{0}L_{Mn^{+2},Mn^{+3}:O^{-2}}^{IONIC\text{-}LIQ} = +1{,}344{,}189 - 803.1101T$

${}^{1}L_{Mn^{+2},Mn^{+3}:O^{-2}}^{IONIC\text{-}LIQ} = -11 + 52.122T$

BCC-A2 (δ-Mn)

2 sublattices, sites 1:3

Constituents Mn, O:Va

$298.15 < T < 1519$

${}^{\circ}G_{Mn:Va}^{HBCC\text{-}A2} - H_{Mn}^{SER} = -3235.3 + 127.85T - 23.7T \ln T - 0.00744271T^2 + 60{,}000T^{-1}$

$1519 < T < 3000$

${}^{\circ}G_{Mn:Va}^{HBCC\text{-}A2} - H_{Mn}^{SER} = -23{,}188.83 + 307.7043T - 48T \ln T + 1.265152 \times 10^{30} T^{-9}$

${}^{\circ}G_{O:Va}^{HBCC\text{-}A2} - H_O^{SER} = +30{,}000 + G(O_2, gas)$

$p = 0.4$

${}^{0}Tc_{Mn:Va}^{BCC\text{-}A2} = -580$

${}^{0}\beta_{Mn:Va}^{BCC\text{-}A2} = -0.27$

CBCC-A12 (α-Mn)

2 sublattices, sites 1:1

Constituents Mn:Va

${}^{\circ}G_{Mn:Va}^{HCBCC\text{-}A12} - H_{Mn}^{SER} = +GH^{SER}(Mn)$

$p = 0.28$

${}^{0}Tc_{Mn:Va}^{CBCC\text{-}A12} = -285$

${}^{0}\beta_{Mn:Va}^{CBCC\text{-}A12} = -0.66$

FCC-A1 (γ-Mn)

2 sublattices, sites 1:1

Constituents Mn,O:Va

$298.14 < T < 1519$

${}^{\circ}G_{Mn:Va}^{FCC\text{-}A1} - H_{Mn}^{SER} = -3439.3 + 131.884T - 24.5177T \ln T - 0.006T^2 + 69{,}600T^{-1}$

$1519 < T < 3000$

${}^{\circ}G_{Mn:Va}^{FCC\text{-}A1} - H_{Mn}^{SER} = -26{,}070.1 + 309.6664T - 48T \ln T - 3.86196 \times 10^{30} T^{-9}$

${}^{\circ}G_{O:Va}^{HFCC\text{-}A1} - H_O^{SER} = +30{,}000 + G(O_2, gas)$

Table II. Cont. Summary of the Parameters Describing the Thermodynamic Properties of the MnO-System (Values are in SI Units)

$p = 0.28$

${}^{0}Tc^{\text{FCC-A1}}_{\text{Mn:Va}} = -1620$

${}^{0}\beta^{\text{FCC-A1}}_{\text{Mn:Va}} = -1.86$

CUB-A13 (β-Mn)

2 sublattices, sites 1:1

Constituents Mn:Va

$298.14 < T < 1519$

${}^{\circ}G^{\text{CUB-A13}}_{\text{Mn:Va}} - H^{\text{SER}}_{\text{Mn}} = -5800.4 + 135.995T - 24.8785T \ln T - 0.00583359T^2 + 70{,}269T^{-1}$

$1519 < T < 3000$

${}^{\circ}G^{\text{CUB-A13}}_{\text{Mn:Va}} - H^{\text{SER}}_{\text{Mn}} = -28{,}290.76 + 311.2933T - 48T \ln T - 3.96757 \times 10^{30}\, T^{-9}$

Halite ($Mn_{1-x}O$)

2 sublattices, sites 1:1

Constituents Mn^{+2}, Mn^{+3}, $Va:O^{-2}$

${}^{\circ}G^{\text{HALITE}}_{\text{Mn}^{+2}:\text{O}^{-2}} - H^{\text{SER}}_{\text{Mn}^{+2}} - H^{\text{SER}}_{\text{O}^{-2}} = +G(\text{MnO})$

${}^{\circ}G^{\text{HALITE}}_{\text{Mn}^{+3}:\text{O}^{-2}} - H^{\text{SER}}_{\text{Mn}^{+3}} - H^{\text{SER}}_{\text{O}^{-2}} = +G(\text{MnO}) - 60{,}498.07 - 20.03189T$

${}^{\circ}G^{\text{HALITE}}_{\text{Va:O}^{-2}} - H^{\text{SER}}_{\text{O}^{-2}} = 0$

${}^{0}L^{\text{HALITE}}_{\text{Mn}^{+2},\text{Mn}^{+3}:\text{O}^{-2}} = +36{,}538.5$

α-Mn_3O_4

2 sublattices, sites 3:4

Constituents Mn:O

${}^{\circ}G^{\text{Mn3O4-ALPHA}}_{\text{Mn:O}} - 3H^{\text{SER}}_{\text{Mn}} - 4H^{\text{SER}}_{\text{O}} = +G(\text{Mn}_3\text{O}_4)$

β-Mn_3O_4

2 sublattices, sites 3:4

Constituents Mn:O

${}^{\circ}G^{\text{Mn3O4-BETA}}_{\text{Mn:O}} - 3H^{\text{SER}}_{\text{Mn}} - 4H^{\text{SER}}_{\text{O}} = +G(\text{Mn}_3\text{O}_4) + 20{,}810 - 14.376047T$

Mn_2O_3

2 sublattices, sites 2:3

Constituents Mn:O

${}^{\circ}G^{\text{Mn2O3}}_{\text{Mn:O}} - 2H^{\text{SER}}_{\text{Mn}} - 3H^{\text{SER}}_{\text{O}} = +G(\text{Mn}_2\text{O}_3)$

MnO_2

2 sublattices, sites 1:2

Constituents Mn:O

${}^{\circ}G^{\text{MnO2}}_{\text{Mn:O}} - H^{\text{SER}}_{\text{Mn}} - 2H^{\text{SER}}_{\text{O}} = +G(\text{MnO}_2)$

Functions:

$298.15 < T < 1000$

$G(O_2, \text{gas}) = -6961.74451 - 76{,}729.7484T^{-1} - 51.0057202T - 22.2710136T \ln T - 0.0101977469T^2 + 1.32369208 \times 10^{-6}\, T^3$

$1000 < T < 3300$

$G(O_2, \text{gas}) = -13{,}137.5203 + 525.809.556T^{-1} + 25.32000332T - 33.627603T \ln T - 0.00119159274T^2 + 1.35611111 \times 10^{-8}\, T^3$

$3300 < T < 6000$

$G(O_2, \text{GAS}) = -27{,}973.4908 + 8{,}766{,}421.4T^{-1} + 62.5195726T - 37.9072074T \ln T - 8.50483772 \times 10^{-4}T^2 + 2.14409777 \times 10^{-8}\, T^3$

$298.15 < T < 1519$

$G(\text{Mn, liq}) = +GH^{\text{SER}}(\text{Mn}) + 17{,}859.91 - 12.6208T - 4.41929 \times 10^{-21}\, T^7$

$1519 < T < 2000$

$G(\text{Mn, liq}) = +GH^{\text{SER}}(\text{Mn}) + 18{,}739.51 - 13.2288T - 1.656847 \times 10^{30}\, T^{-9}$

$298.14 < T < 1519$

$GH^{\text{SER}}(\text{Mn}) = -8115.28 + 130.059T - 23.4582T \ln T - 0.00734768T^2 + 69{,}827T^{-1}$

$1519 < T < 2000$

$GH^{\text{SER}}(\text{Mn}) = -28{,}733.41 + 312.2648T - 48T \ln T + 1.656847 \times 10^{30}\, T^{-9}$

$G(\text{MnO, liq}) = -252{,}595 - 293.164T + 15.0712T \ln T$

$G(\text{MnO}) = -401{,}784.4 + 268.75251T - 48.2744592T \ln T - 0.003230661T^2 + 257{,}553.188T^{-1}$

$G(\text{Mn}_3\text{O}_4) = -1{,}443{,}167 + 905.71T - 156.211772T \ln T - 0.0179602213T^2 + 1{,}106{,}277.72T^{-1}$

$G(\text{Mn}_2\text{O}_3) = -993{,}634.5 + 584.605647T - 102.148721T \ln T - 0.0181244679T^2 + 595{,}113T^{-1}$

$G(\text{MnO}_2) = -548{,}242 + 444.10228T - 72.5000062T \ln T - 0.002720343T^2 + 885{,}523.74T^{-1}$

Table III. Invariant Equilibria in the Assessed Mn-O System at 0.21 Atm

Reaction	Mole Fraction O in the Respective Phases			Temperature (K) Calculated	Temperature (K) Experimental
L1 = δ − Mn + $Mn_{1-x}O$	1.46×10^{-3}	2.005×10^{-3}	0.5	1515	1515[2,3]
L2 = L1 + $Mn_{1-x}O$	3.65×10^{-11}	0.4886	0.5	2063	2063[2]
$Mn_{1-x}O$ = L2	0.5	0.5	—	2123	2123[2,4]
L2 = $Mn_{1-x}O$ + β − Mn_3O_4	0.5419	0.5275	0.5714	1833	1833[2]
β-Mn_3O_4 = L2 + Gas	0.5714	0.5441	1	1846	1853,[2] 1840[5]
Mn_2O_3 = α-Mn_3O_4 + Gas	0.6	0.5714	1	1161	1162[39]
MnO_2 = Mn_2O_3 + Gas	0.6667	0.6	1	697	694[40]
α-Mn_3O_4 = β-Mn_3O_4	0.5714	0.5714	—	1448	1445[20,23,32,33]
γ-Mn = δ-Mn	0	0	—	1383	—
β-Mn = γ-Mn	0	0	—	1360	—

Table IV. The Assessed and Reported Values of $\Delta°H_{298}$ and $°S_{298}$

Compounds	Calculated $\Delta°H_{298}$(KJ/mol)	Reported $\Delta°H_{298}$(KJ/mol)	Calculated $°S_{298}$(J/mol/K)	Reported $°S_{298}$(J/mol/K)
$Mn_{1-x}O$	−385.2	−385.2[20]	59.5	59.9[20]
α-Mn_3O_4	−1387.6	−1387.6[20]	163.7	164.1,[30] 154[20]
Mn_2O_3	−957.6	−957.6[20]	117.0	113.7,[30] 110.5[20]
MnO_2	−520.4	−520.4[20]	53.1	52.8,[30] 53.2[20]

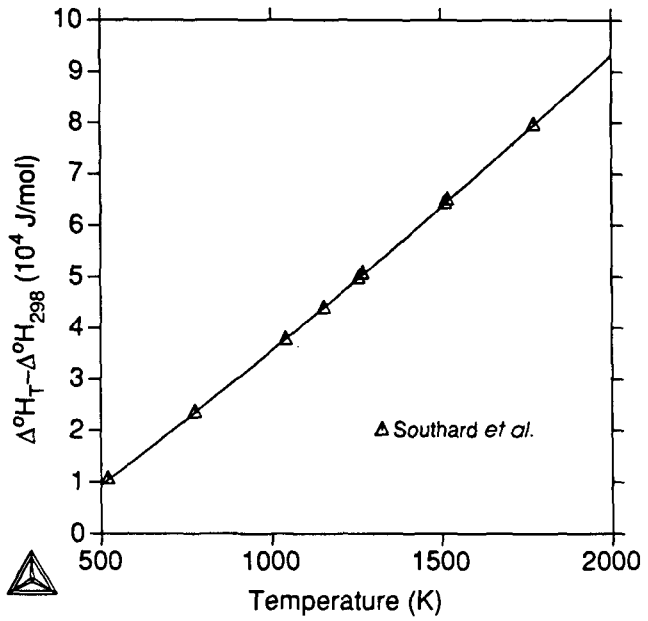

Fig. 2—Calculated *vs* experimental heat content of manganosite.

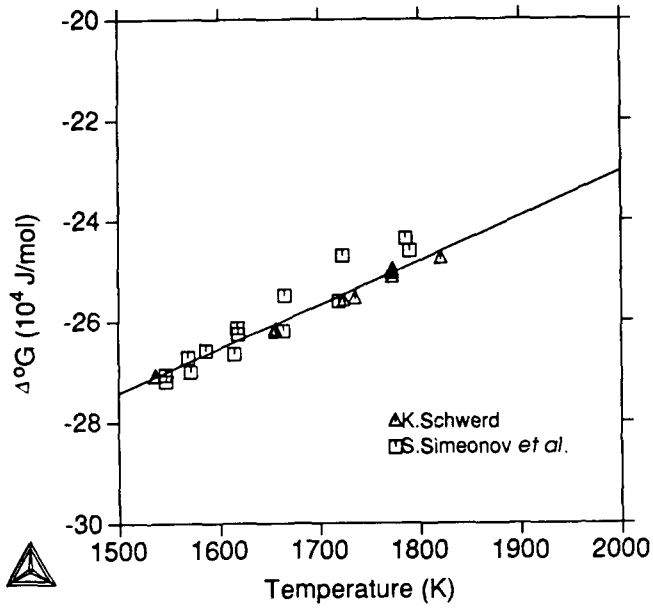

Fig. 3—Calculated *vs* experimental Gibbs energy of formation of manganosite.

Picard and Gerdanian.[12] Expressed in oxygen content, the deviations are within the experimental uncertainty. In Figure 4(b), other experimental data are shown, together with the calculated curves. As already mentioned, there are large discrepancies among the reported data. It is suspected that the reliability of the experimental technique and the extreme difficulty in attaining of equilibrium in this system are the main reasons for the discrepancies. Figure 5 shows the oxygen solubility in the manganosite phase compared with the experimental data by Fender and Riley.[15]

B. *Hausmanite*

The assessment of the Gibbs energy of formation of the hausmanite was based on the evaluated parameters of manganosite phase and the selected experimental data. The parameters are given in Table II. Figures 6 and 7 show the calculated heat capacity and enthalpy varying with temperature, both of which have been fitted well to the experimental data. The oxygen potential is presented in Figure 8 in comparison with the experimental data by many authors.[22–29] The calculated temperature (T = 1448 K) and enthalpy (ΔH = 20,810 J/mol) of the

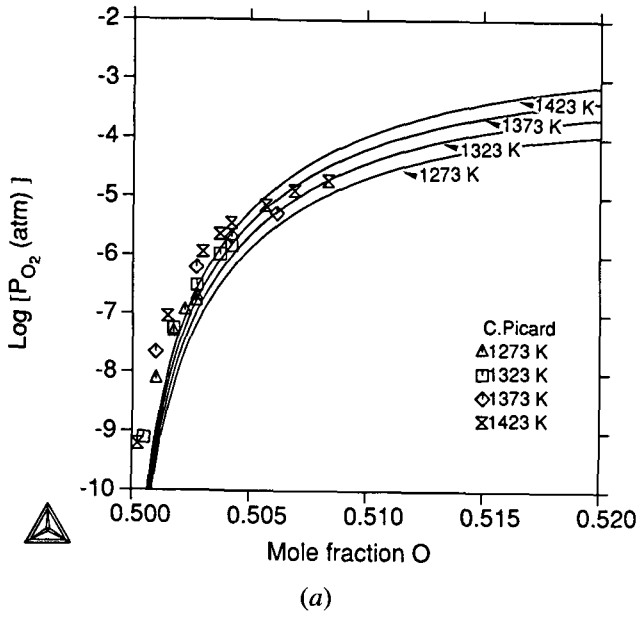

(*a*)

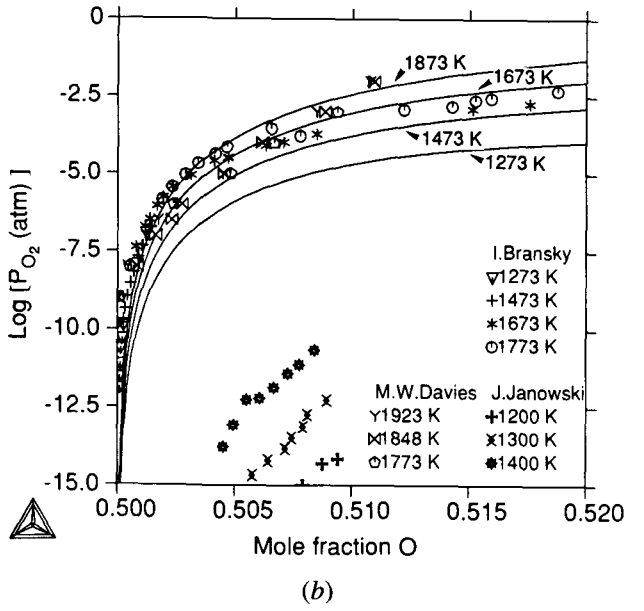

(*b*)

Fig. 4—(*a*) Calculated oxygen activity in manganosite *vs* experimental data used in the optimization and (*b*) calculated oxygen activity in manganosite *vs* other experimental data which were not used in the optimization.

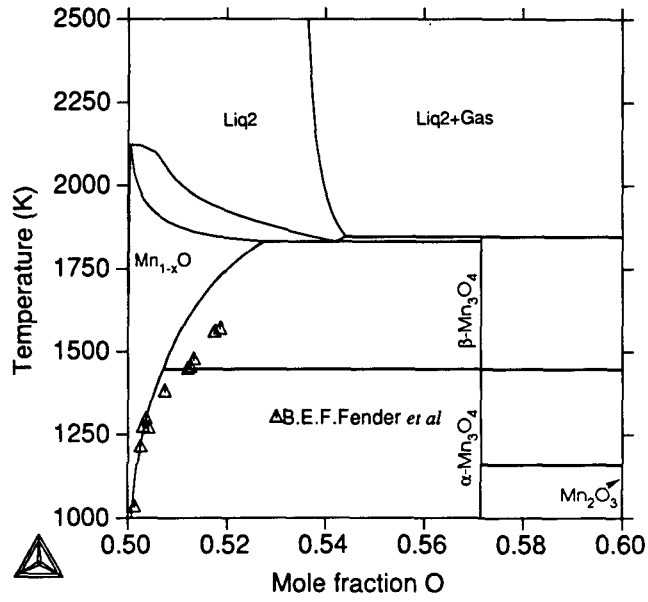

Fig. 5—Calculated oxygen solubility in manganosite with experimental data.

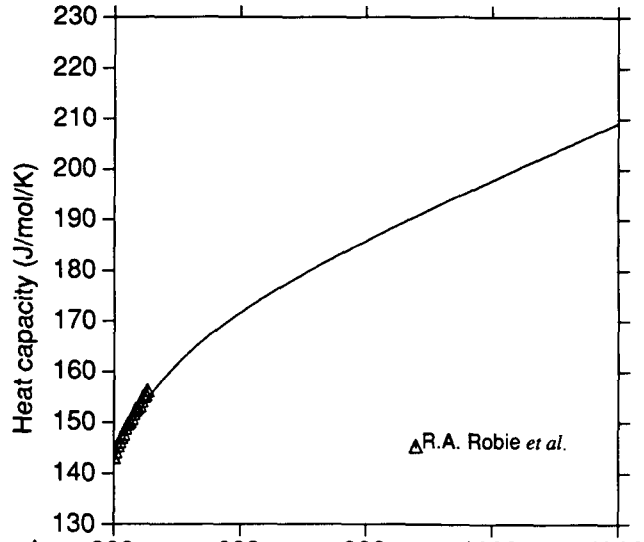

Fig. 6—Calculated *vs* experimental heat capacity of hausmanite (Mn_3O_4).

structural transformation of hausmanite also fit with the selected data well.

C. *Liquid Phase*

With the parameters of solid phases evaluated, the parameters of the liquid phase were optimized to fit all the invariant equilibria and the miscibility gap. More attention was paid to fit the temperatures rather than the compositions. The calculated temperatures of the invariant equilibria are listed in Table III, compared with the values reported. The calculated oxygen solubility in liquid manganese fits well with the experimental data measured by Jacob[45] and Simeonov *et al.*,[17] as shown in Figure 9, close to pure manganese.

D. *Bixbyite*

With the parameters of the hausmanite phase and the experimental information, the Gibbs energy of the bixbyite phase was evaluated with five parameters. The calculated heat capacity, heat content, and oxygen potential *vs* temperature are shown in Figures 10 through 12. In

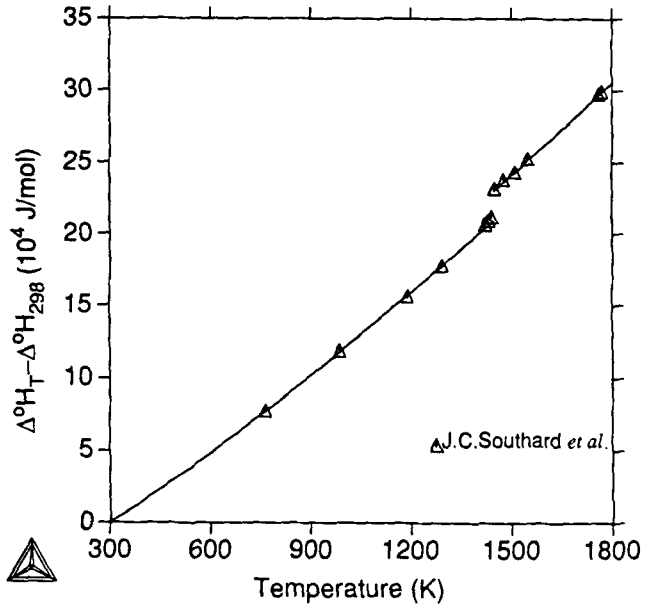

Fig. 7—Calculated *vs* experimental heat content of hausmanite (Mn_3O_4).

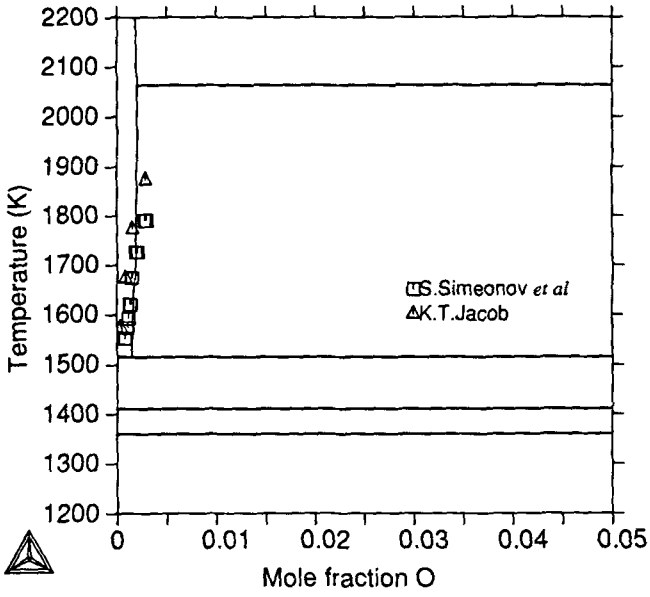

Fig. 9—Calculated *vs* experimental oxygen solubility in liquid manganese.

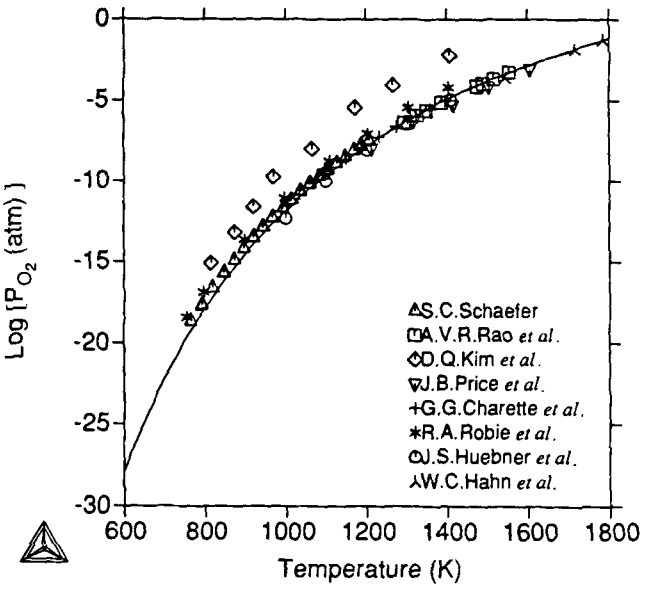

Fig. 8—Calculated *vs* experimental oxygen potential of hausmanite (Mn_3O_4).

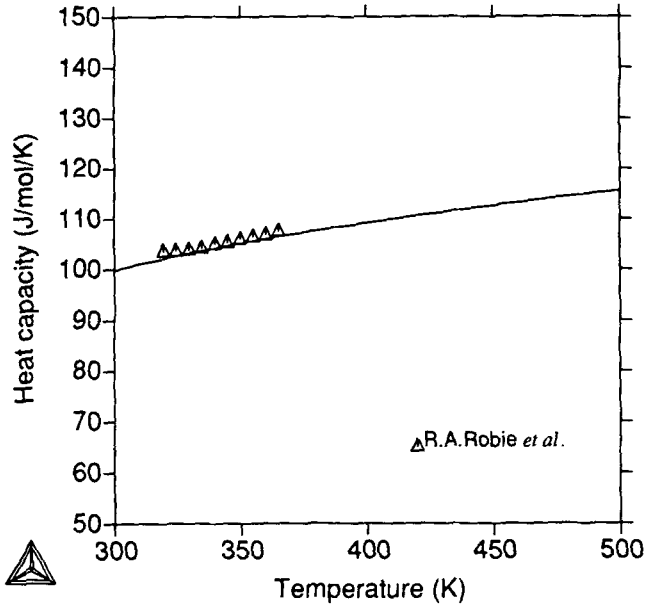

Fig. 10—Calculated *vs* experimental heat capacity of bixbyite (Mn_2O_3).

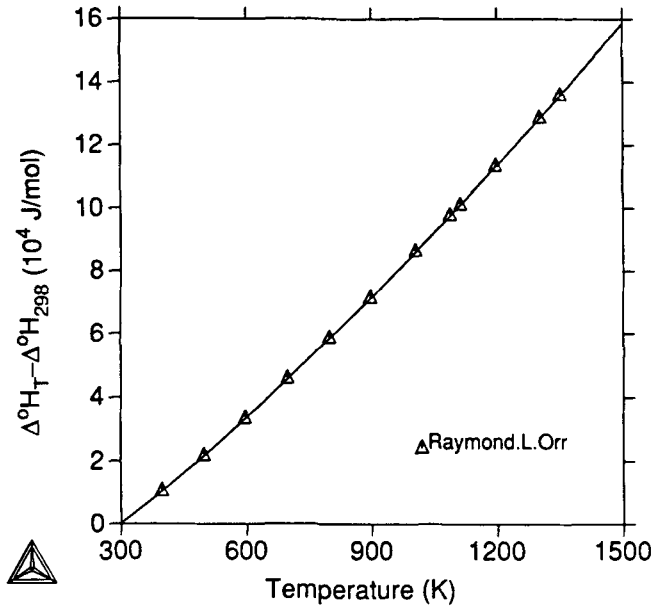

Fig. 11—Calculated *vs* experimental heat content of bixbyite (Mn_2O_3).

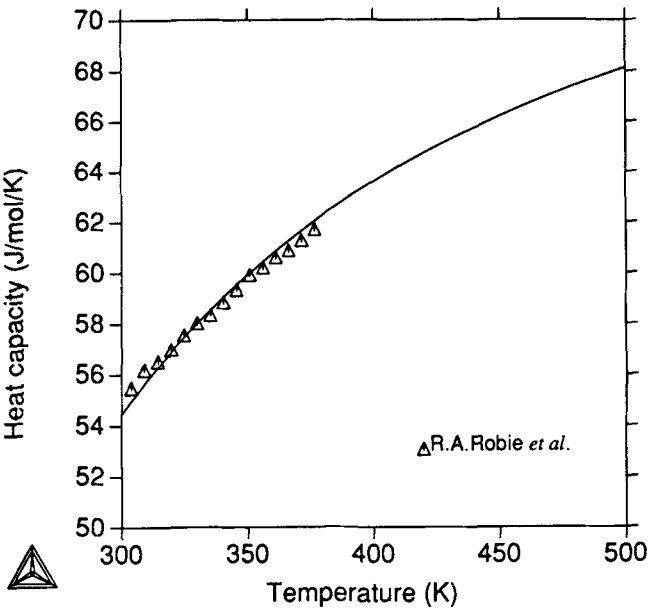

Fig. 13—Calculated *vs* experimental heat capacity of pyrolusite (MnO_2).

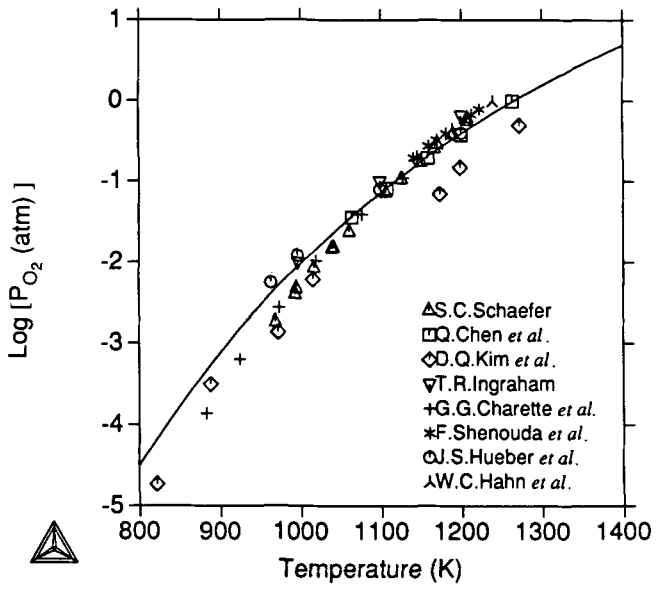

Fig. 12—Calculated *vs* experimental oxygen potential of bixbyite (Mn_2O_3).

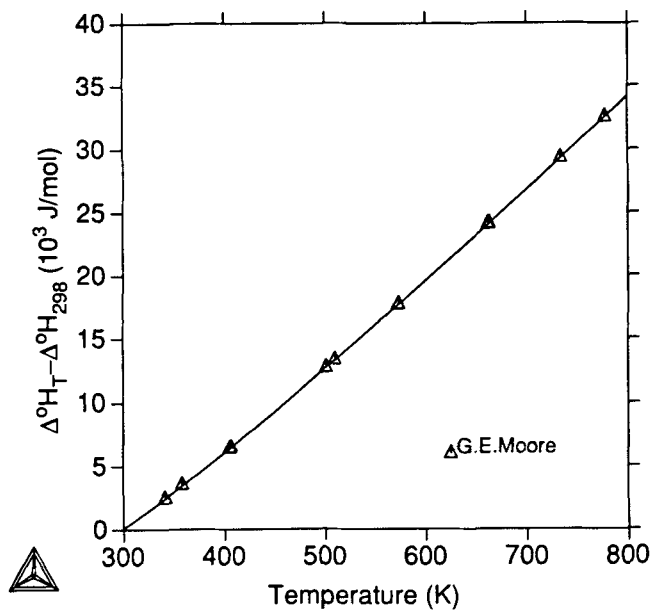

Fig. 14—Calculated *vs* experimental heat content of pyrolusite (MnO_2).

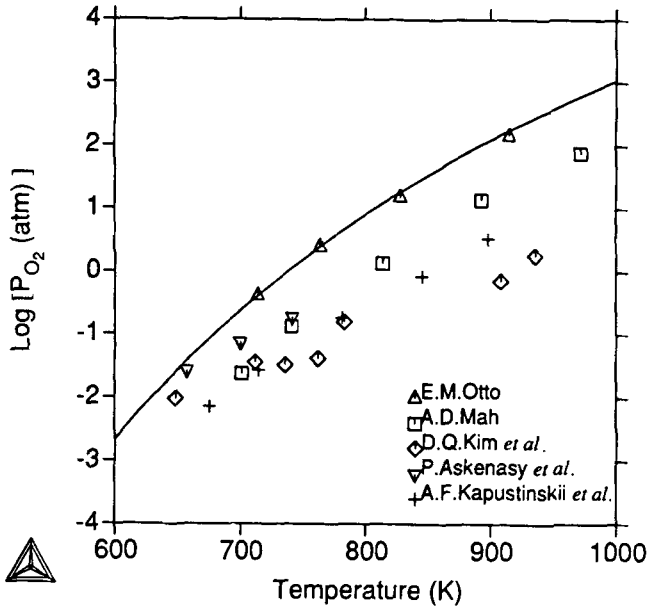

Fig. 15—Calculated *vs* experimental oxygen potential of pyrolusite (MnO_2).

Figure 12, other experimental data by Kim *et al.*,[25] Ingraham,[54] Charette and Flengas,[26] Shenouda and Aziz,[55] and Hahn and Muan,[29] which were not used in the optimization, are also included. Good agreement between the calculation and the experimental data can be observed.

E. *Pyrolusite*

The Gibbs energy of pyrolusite was finally assessed based on the selected experimental data, and the results are shown in Figures 13 through 15 for the heat capacity, heat content, and oxygen potential. The present description of the Gibbs energy of the pyrolusite phase reproduces well the experimental data of the heat capacity by Robie and Hemingway,[30] the heat content by Moore,[44] and the oxygen potential only by Otto.[40] The other experimental results obtained from the decomposition oxygen pressure may be less reliable, as discussed earlier.

V. SUMMARY AND CONCLUSIONS

The present thermodynamic evaluation of the Mn-O system has been made by using thermodynamic models for the Gibbs energy of individual phases. An optimized set of thermodynamic parameters has been obtained on the consideration of related experimental information. For the solid manganese oxides, the parameters of the Gibbs energy have been revised by considering all the available thermodynamic information. Due to the scarce and inconsistent experimental information on some phases, there are some uncertainties in the evaluation of thermodynamic properties still remaining, particularly for the liquid phase. However, with the present assessment, a basic thermodynamic description of the Mn-O system is provided which permits extrapolations and can be included in the description of the higher order systems.

ACKNOWLEDGMENTS

One of the authors (M. Wang) wishes to thank many colleagues of Thermo-Calc group, particularly Mr. Caian Qiu, for the valuable discussion and help received during this work. Some useful comments on the manuscript by Professor Mats Hillert and Dr. Zikui Liu are also appreciated. Our work was financially supported by the Division of Physical Metallurgy of the Royal Institute of Technology and the bilateral scholarship between the Swedish and Chinese governments.

REFERENCES

1. T.B. Massalski, H. Okamoto, P.R. Subramanian, and L. Kacprzak: *Binary Alloy Phase Diagrams*, 2nd ed., ASM INTERNATIONAL., Metals Park, OH, 1990, vol. 3, pp. 2583-85.
2. G. Trömel, W. Fix, K. Koch, and F. Schaberg: *Erzmetall.*, 1976, vol. 29, pp. 234-37.
3. Q. Chen: *Acta Metall. Sinica*, 1988, vol. 24, pp. B440-41.
4. A.Z. Hed and D.S. Tannhauser: *J. Electrochem. Soc.*, 1967, vol. 114, pp. 314-18.
5. K.J. Tauer and R.J. Weiss: *J. Phys. Chem. Solids*, 1957, vol. 2, p. 237-43.
6. R.J. Weiss and K.J. Tauer: *J. Phys. Chem. Solids*, 1958, vol. 4, pp. 135-43.
7. R. Hultgren, P.D. Desai, D.T. Hawkins, M. Gleiser, K.K. Kelley, and D.D. Wagman: *Selected Values for the Thermodynamic Properties of the Elements*, ASM, Metals Park, OH, 1973, pp. 301-08.
8. M. Hillert: *Trita-Mac-0305 (revised)*, Royal Institute of Technology, Stockholm, Sweden, Feb. 1986.
9. P.D. Desai: *J. Phys. Chem. Ref. Data*, 1987, vol. 16, p. 91.
10. A.F. Guillermet and W. Huang: *Int. J. Thermophys.*, 1990, vol. 11, pp. 949-69.
11. M.W. Davies and F.D. Richardson: *Trans. Faraday Soc.*, 1959, vol. 55, pp. 604-10.
12. C. Picard and P. Gerdanian: *J. Solid State Chemistry*, 1974, vol. 11, pp. 190-202.
13. I. Bransky and N.M. Tallan: *J. Electrochem. Soc.*, 1971, vol. 118, pp. 788-93.
14. J. Janowski, R. Benesch, M. Jaworski, and A. Miklasinski: *Zesz. Nauk. Akad. Gorn.-Hutn. Stanislaw Staszica*, 1974, vol. 437, pp. 49-68.
15. B.E.F. Fender and F.D. Riley: *Chem. Extended Defects Non-Metal Solids*, Proc. Institute for Advanced Study, LeRoy Eyring, eds., North-Holland Publishing Co., Amsterdam, 1970, pp. 54-61.
16. K. Schwerdtfeger: *Trans. TMS-AIME*, 1967, vol. 239, pp. 1276-81.
17. S. Simeonov, I. Ivanchev, and D. Popivanov: *Izv. Vyssh. Uchebn. Zaved. Chern. Metall.*, 1990, vol. 11, pp. 20-22.
18. J. Kleinclauss, R. Mainard, H. Fousse, N. Ciret, D. Bour, and A.J. Pointon: *J. Phys. C: Solid State Phys.*, 1981, vol. 14, pp. 1163-77.
19. J.C. Southard and C.H. Shomate: *J. Am. Chem. Soc.*, 1942, vol. 64, pp. 1770-74.
20. O. Kubaschewski, E.L.L. Evans, and C.B. Alcock: *Metallurgical Thermochemistry*, 5th ed., Pergamon Press, New York, NY, 1979, p. 294.
21. V. Raghavan: *Phase Diagrams of Ternary Iron Alloys, Part 5*, The Indian Institute of Metals, Calcutta, 1989, p. 183.
22. S.C. Schaefer: United States Department Interior, Bureau of Mines, Washington, DC, Rep. Invest., 1982, no. 8704.
23. A.V. Ramana Rao and V.B. Tare: *Inst. Min. Metall., Bull. Trans., G.B.*, 1973, vol. 82 (796), pp. 34-37.
24. J.B. Price and J.B. Wagner: *J. Electrochem. Soc.*, 1970, vol. 117 (2), pp. 242-47.
25. D.Q. Kim, Y. Wilbert, and F. Marion: *C.R. Acad. Sc. Paris (C)*, 1966, vol. 262, pp. 756-58.
26. G.G. Charette and S.N. Flengas: *J. Electrochem. Soc.*, 1968, vol. 115, pp. 796-804.
27. R.A. Robie and D.R. Waldbaum: *U.S. Geol. Survey Bull.*, 1968, vol. 1259, p. 256.

28. J.S. Huebner and M. Sato: *Am. Mineral.*, 1970, vol. 55, pp. 934-42.
29. W.C. Hahn and A. Muan: *Am. J. Sci.*, 1960, vol. 258 (1), pp. 60-78.
30. R.A. Robie and B.S. Hemingway: *J. Chem. Thermodyn.*, 1985, vol. 17 (2), pp. 165-81.
31. J.C. Southard and G.E. Moore: *J. Am. Chem. Soc.*, 1942, vol. 64, pp. 1769-70.
32. N.G. Schmahl and B. Stemmler: *J. Electrochem. Soc.*, 1965, vol. 112, p. 365.
33. J.F. Elliot and M. Gleiser: *Thermochemistry for Steelmaking*, Addison-Wesley, Reading, MA, 1960, vol. 1, p. 296.
34. H.F. McMurdie and E. Golovato: *N.B.S. J. Res.*, 1948, vol. 41, pp. 589-600.
35. H.J. Van Hook and M.L. Keith: *Am. Mineralogist*, 1958, vol. 43, pp. 69-83.
36. P. Dubois: *Compt. Rend.*, 1934, vol. 199, pp. 1416-18.
37. B. Masson: *Geol. Fr. Stockholm Forh.*, 1943, vol. 65, pp. 97-180.
38. R.L. Orr: *J. Am. Chem. Soc.*, 1954, vol. 76, pp. 857-58.
39. Q. Chen and X. Chen: *J. Central-South Inst. Mining Metall.* (in Chinese), 1982, no. 3, pp. 1-9.
40. E.M. Otto: *J. Electrochem. Soc.*, 1965, vol. 112, p. 367.
41. A.D. Mah: *U.S. Bur. Mines Repts. Invest.*, 1960, no. 5600.
42. P. Askenasy and S. Klonowski: *Z. Elektrochem.*, 1910, vol. 16, p. 104.
43. A.F. Kapustinskii and K.C. Bayuskhina: *Zhur. Fiz. Khim. (USSR)*, 1938, vol. 11, p. 77.
44. G.E. Moore: *J. Am. Chem. Soc.*, 1943, vol. 65, pp. 1398-99.
45. K.T. Jacob: *Metall. Trans. B*, 1981, vol. 12B, pp. 675-78.
46. M. Hillert and L.-I. Staffansson: *Acta Chem. Scand.*, 1970, vol. 24, pp. 3618-26.
47. M. Hillert, B. Jansson, and B. Sundman: *Z. Metallkd.*, 1988, vol. 79, pp. 81-87.
48. B. Sundman: *CALPHAD*, 1991, vol. 15 (2), pp. 109-19.
49. M. Hillert, B. Jansson, B. Sundman, and J. Ågren: *Metall. Trans. A*, 1985, vol. 16A, pp. 261-66.
50. B. Sundman: *J. Phase Equilibria*, 1991, vol. 12 (1), pp. 127-40.
51. M. Hillert, M. Selleby, and B. Sundman: *Metall. Trans. A*, 1990, vol. 21A, pp. 2759-76.
52. B. Jansson: Thesis, Royal Institute of Technology, Stockholm, Sweden, 1984.
53. B. Sundman, B. Jansson, and J.O. Andersson: *CALPHAD*, 1985, vol. 9, pp. 153-90.
54. T.R. Ingraham: *Can. Metall. Q.*, 1966, vol. 5 (2), pp. 109-21.
55. F. Shenouda and S. Aziz: *J. Appl. Chem.*, 1967, vol. 17, Sept., pp. 258-62.